Hindawi Publishing Corporation
Journal of Nanomaterials
Volume 2011, Article ID 495676, 18 pages
doi:10.1155/2011/495676

Research Article

Surface Modification Effects on CNTs Adsorption of Methylene Blue and Phenol

A. H. Norzilah,[1] A. Fakhru'l-Razi,[1,2] Thomas S. Y. Choong,[1] and A. Luqman Chuah[1,3]

[1] *Department of Chemical and Environmental Engineering, Universiti Putra Malaysia, 43400 Serdang, Malaysia*
[2] *Institute of Advanced Technology (ITMA), Universiti Putra Malaysia, 43400 Serdang, Malaysia*
[3] *Institute of Tropical Forestry and Forest Product (INTROP), Universiti Putra Malaysia, 43400 Serdang, Malaysia*

Correspondence should be addressed to A. Fakhru'l-Razi, fakhrul@eng.upm.edu.my

Received 18 March 2011; Revised 13 June 2011; Accepted 8 July 2011

Academic Editor: Sherine Obare

This study compares the adsorption capacity of modified CNTs using acid and heat treatment. The CNTs were synthesized from acetone and ethanol as carbon sources, using floating catalyst chemical vapor deposition (FC-CVD) method. energy-dispersive X-ray spectroscopy (EDX) and Boehm method revealed the existence of oxygen functional group on the surface of CNTs. Heat modification increases the adsorption capacity of as-synthesized CNTs for methylene blue (MB) and phenol by approximately 76% and 50%, respectively. However, acid modification decreases the adsorption capacity. The equilibrium adsorption data fitted the Redlich-Peterson isotherm. For the adsorption kinetic study, the experimental data obeyed the pseudo-second-order model. Both modifications methods reduced the surface area and pore volume. The studies show that the adsorption of MB and phenol onto modified CNTs is much more influenced by their surface functional group than their surface area and pore volume.

1. Introduction

The effluent discharged from the textile industry contains mainly dyes. Dyes can cause allergic dermatitis and skin irritation [1]. High amount of dyes releases into water surface causes abnormal coloration and has bad effect on the growth of bacteria and biological activity [2]. Some are reported to be carcinogenic and mutagenic for aquatic organisms [3]. Phenolic compounds are discharged from the coal tar, gasoline, plastic, rubber proofing, disinfectant, pharmaceutical and steel industries, domestic wastewaters, agricultural runoff, and chemical spills industries. The presence of phenolic compounds even at low concentration can cause unpleasant taste and odour. Adsorption is a promising method for wastewater treatment compared to the other methods such as precipitation and coagulation [4], chemical oxidation [5], sedimentation [6], filtration [7], osmosis, and ion exchange [8]. The method is recognized for its high efficiency, low cost, simplicity, reusability of the adsorbent, and easy recovery. One of the most recent studied materials is carbon nanotubes (CNTs).

CNTs are made up of concentric rolled graphene sheets produced from laser ablation, chemical vapor deposition, and arc discharge. CNTs have been used as gas sensor [26], nanofiber-reinforcing composites [27], paper batteries [28], solar cells [29], and supercapacitors [30], due to their excellent electrical, electronic, and mechanical properties. Their high surface area, small diameter, various bulks and individual morphology plus their defected and easily functionalized surface are beneficial for CNTs to become a potential adsorbent for liquid adsorption. CNTs have been used as adsorbents for different types of pollutants such as inorganic pollutant (Cu(II) [31], Cr (VI) [32], and Zn(II) [33] and organic pollutant (methylene blue [16], natural organic matter (NOM) [34], and nitroaromatic compunds [24].

Surface functional groups play an important role in adsorption. Functional groups commonly found on the surface of as-prepared CNTs are carboxylic, lactonic, carbonyl, and hydroxyl [24, 31, 35, 36]. The quantity of the functional group on the external and internal surface of CNTs surface can be increased or be reduced by suitable surface treatment

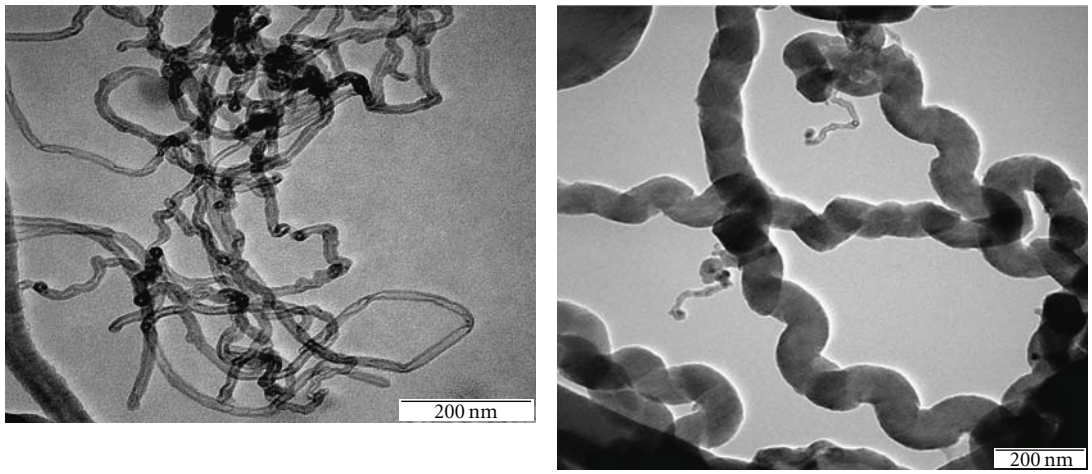

Figure 1: TEM images of (a) CNT-A-HM and (b) CNT-E-HM.

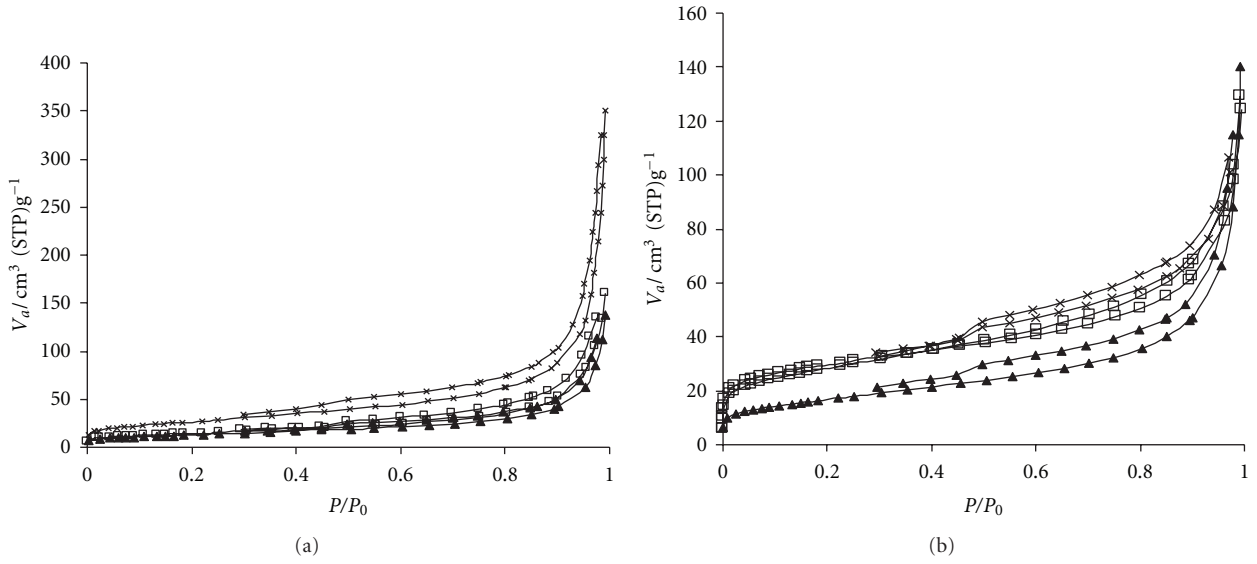

Figure 2: N_2 adsorption isotherms of (a) CNT-A and (b) CNT-E at 77 K: □ CNT-A-AM; ▲ CNT-A-HM; × CNT-A (as synthesized); □ CNT-E-AM; ▲ CNT-E-HM; × CNT-E (as synthesized).

Table 1: Structures and characteristics of MB and phenol.

Name	Molecular size width (nm) × Length (nm) × thickness (nm)	Formula	Molecular weight (g/mol)	λ_{max} (nm)	Molecular structure
MB	0.740 × 1.690 × 0.380	$C_{16}H_{18}ClN_3S$	319.85	664	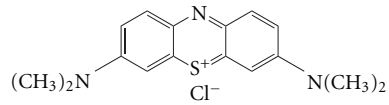
phenol	0.638× 0.792 × 0.822	C_6H_6O	94.11	270	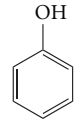

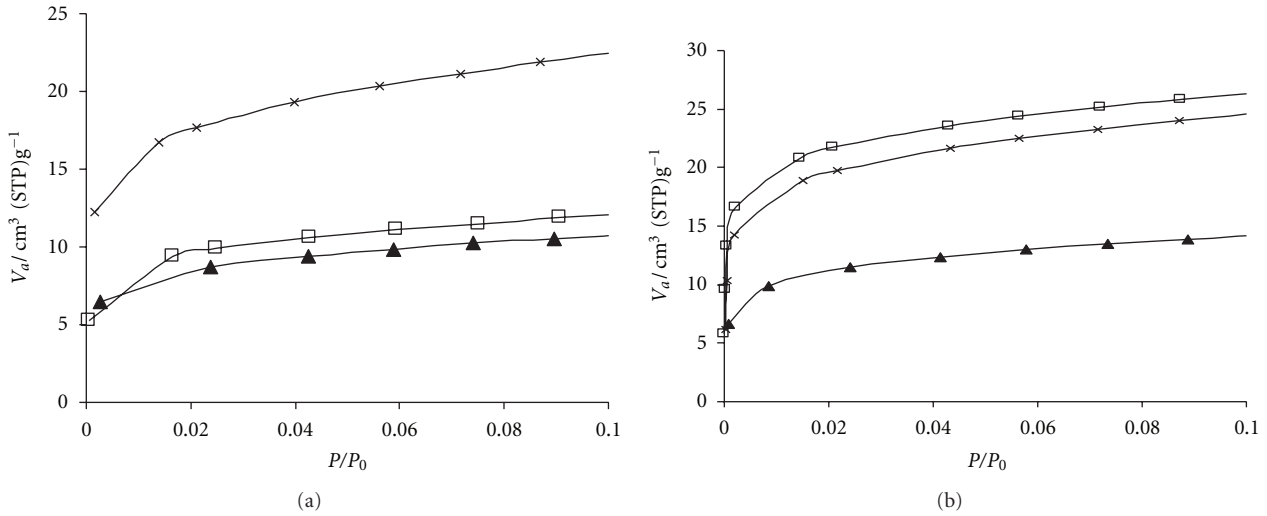

Figure 3: Extended region of low $P/P_0 < 0.1$; (a) CNT-A; (b) CNT-E: □ CNT-A-AM; ▲ CNT-A-HM; × CNT-A (as synthesized); □ CNT-E-AM; ▲ CNT-E-HM; × CNT-E (as synthesized).

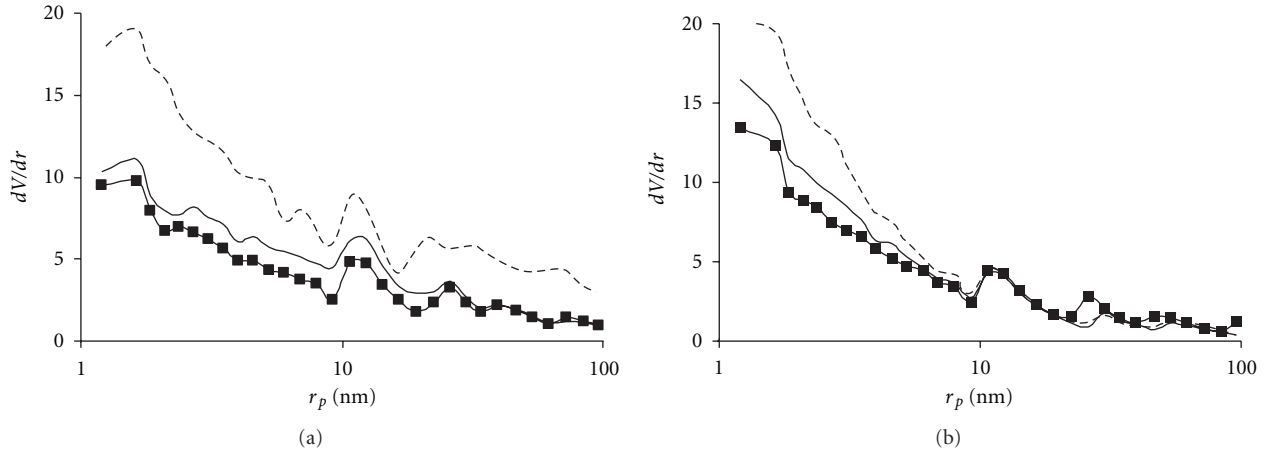

Figure 4: Pore size distributions of (a) CNT-A and (b) CNT-E; — CNT-A-AM; ■ CNT-A-HM; - - - - CNT-A (as synthesized); — CNT-E-AM; ■ CNT-E-HM; - - - - CNT-E (as synthesized).

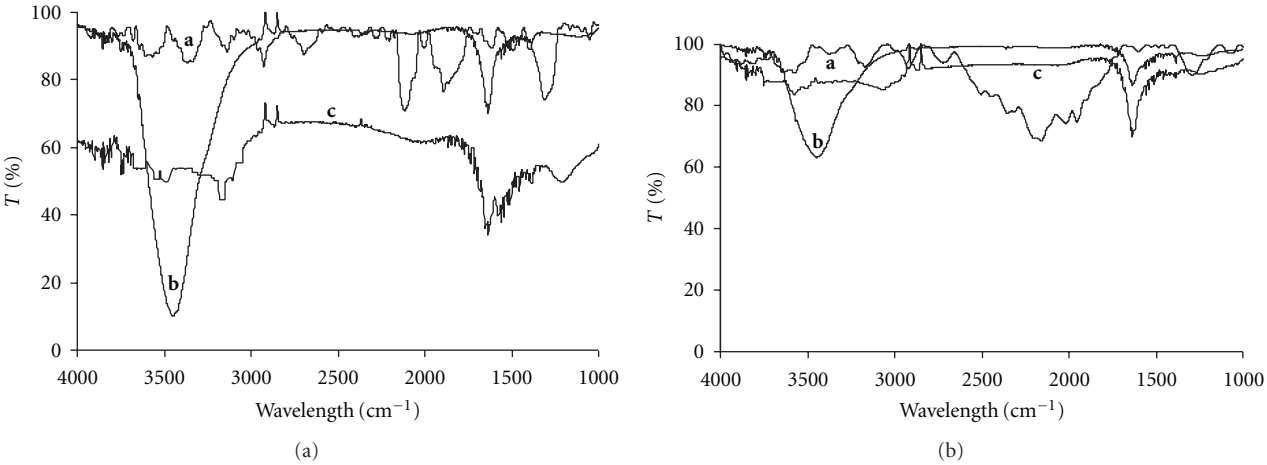

Figure 5: FTIR Spectra of (a) CNT-A: **a**—CNT-A (as synthesized); **b**—CNT-A-AM; **c**—CNT-A-HM; (b) CNT-E: **a**—CNT-A (as synthesized); **b**—CNT-A-AM; **c**—CNT-A-HM.

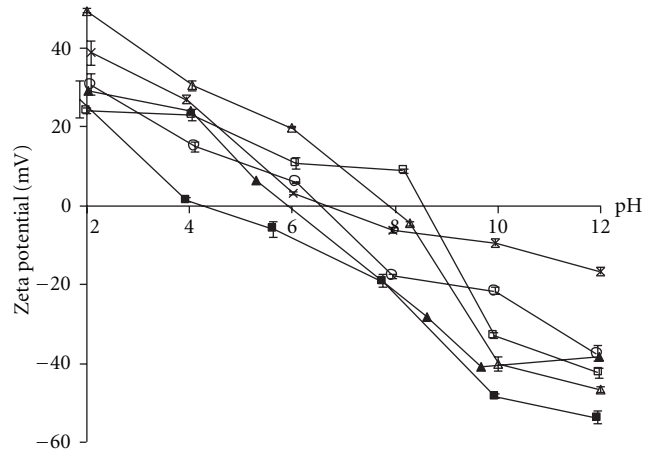

Figure 6: Zeta potential of modified and as-synthesized CNTs: × CNT-A (as synthesized); △ CNT-A-HM; ▲ CNT-A-AM; ◯ CNT-E (as synthesized); □ CNT-E-HM; ■ CNT-E-AM. Each point is the average value of triplicate samples. Error bars represent the range.

Table 2: Physical properties of CNTs.

CNTs	BET surface area (m^2/g)	Total pore Volume (cm^3/g)	Purity (%)*
CNT-A (As synthesized)	90.429	0.4986	93.51
CNT-E (As synthesized)	89.159	0.1729	94.89
CNT-A-HM	43.776	0.2026	92.95
CNT-A-AM	49.976	0.2339	95.65
CNT-E-HM	55.392	0.1866	94.68
CNT-E-AM	86.741	0.1803	97.46

* Determined by TGA; purity = 100% − residue (%).

Table 3: Elemental composition of CNTs.

CNTs	C (wt%)	Fe (wt%)	O (wt%)
CNT-A (as synthesized)	86.87	12.68	0.45
CNT-E (as synthesized)	90.51	8.64	0.85
CNT-A-HM	94.65	5.26	0.09
CNT-A-AM	91.58	5.89	2.53
CNT-E-HM	91.40	8.12	0.48
CNT-E-AM	90.89	6.20	2.91

[37]. The functional groups were attributed to influence significantly the adsorption capacity of resorcinol on MWCNTs [25] and *o*-xylene and *p*-xylene on SWCNTs.

Heat modification using argon is shown to be beneficial for producing high crystallinity and uniformity of carbon's surface [21, 38]. However, very few investigations were reported on the adsorption of organic pollutant onto heat-modified CNTs, except the negative effect of graphitized CNTs on adsorption of 1,2-dichlorobenzene [39].

In this study, heat-modified and acid-modified CNTs were used for the adsorption of methylene blue (MB) and phenol. The objective of this study was to compare the adsorption capacity of heat-modified and acid-modified CNTs. The adsorption equilibrium was fitted by Langmuir, Freundlich, and Redlich-Peterson models. The adsorption kinetic was tested by pseudo-first-order kinetic, pseudo second-order kinetic and intraparticle diffusion model.

2. Materials and Method

2.1. Chemicals. MB (purity ≥ 98.5%, HmbG chemicals) and phenol (purity ≥ 99%, Sigma-Aldrich) were used as received. Other chemicals such as sodium hydroxide (NaOH), hydrochloric acid (HCl), sodium carbonate (Na_2CO_3) and sodium bicarbonate ($NaHCO_3$), were purchased as analytical reagent. All solutions used in the experiment were prepared using distilled water.

2.2. CNTs Preparation. Two types of CNTs with different morphologies were produced by FC-CVD method using acetone and ethanol as carbon sources. The CNTs were synthesized using an apparatus consisting of a ceramic tube (50 mm OD, 40 mm ID, and 1 m long) located horizontally inside a furnace with two stages. The first stage was a quartile of a tube wrapped using heating tape in order to heat the catalyst up to 150°C. The second stage was an electrical furnace (carbolite) equipped with silicon carbide heating element that could be heated up to 1200°C, with 10°C/min heating rate.

After the temperature at the second stage was maintained at 700°C for about 1 hour, the temperature of the first stage (where ferrocene was located ~500 mg) was raised to 150°C. At this step, argon flow (75 mL/min) was stopped to avoid Fe nanoparticles being flown out of the first stage. Then after 3 minutes, hydrogen was bubbled into the carbon sources at flow rate of 150 and 100 mL/min for CNT-A and CNT-E, respectively. The first stage of the reactor was maintained at 150°C during the reaction for 3–5 hours. After the synthesis, the CNTs were cooled to room temperature in argon flow. Finally, the as synthesized CNTs were heated by air oxidation at 350°C for 1 hour to remove amorphous carbon [40].

Table 4: Boehm titration method.

CNTs	Carboxyl (mmol/g)	Lactones (mmol/g)	Phenols (mmol/g)	Total acidity (mmol/g)	Total basicity (mmol/g)
CNT-A (as synthesized)	0.1680	0.1530	0.3970	0.7188	0.0199
CNT-E (as synthesized)	0.1970	0.0590	0.4640	0.7200	0.0192
CNT-A (AM)	0.2519	0.1963	0.5931	1.0413	0.0144
CNT-A (HM)	0.0123	0.0139	0.0176	0.0438	0.0562
CNT-E (AM)	0.2774	0.1705	0.5621	1.0100	0.0164
CNT-E (HM)	0.0226	0.0250	0.0061	0.0538	0.0616

Table 5: The coefficients of the Langmuir, Freundlich, and Redlich-Peterson isotherms for MB system.

(a)

CNTs	Langmuir isotherm			
	Q_m (mmol/kg)	K_L (L/mmol)	R_L (−)	R^2
CNT-A (as synthesized)	84.66	595.30	0.0138	0.9914
CNT-E (as synthesized)	103.86	8433.29	0.0009	0.9998
CNT-A-AM	80.09	1779.68	0.0039	0.9309
CNT-E-AM	99.83	2085.33	0.0036	0.9442
CNT-A-HM	93.15	2171.75	0.0036	0.9870
CNT-E-HM	182.71	2594.46	0.0057	0.9402

(b)

CNTs	Freundlich isotherm			
	K_F (mmol/kg)/(mmol/L)$^{1/n}$	n (−)	$1/n$	R^2
CNT-A (as synthesized)	138.31	5.28	0.1895	0.9624
CNT-E (as synthesized)	134.55	10.64	0.0940	0.6392
CNT-A-AM	112.77	7.63	0.1310	0.9017
CNT-E-AM	142.32	7.36	0.1358	0.9034
CNT-A-HM	144.34	6.02	0.1662	0.9020
CNT-E-HM	335.04	5.58	0.1793	0.8621

(c)

CNTs	Redlich-Peterson				
	A_R (L/g)	B_R (L/mmol)	q_{R-P} (mmol/kg)	β_R (−)	R^2
CNT-A (as synthesized)	51.10	609.38	83.86	0.9970	0.9915
CNT-E (as synthesized)	1259.21	11955.74	105.32	0.9980	0.8738
CNT-A-AM	241.88	3679.08	65.74	0.9350	0.9979
CNT-E-AM	276.29	3193.16	86.52	0.9530	0.9976
CNT-A-HM	403.62	5893.01	68.49	0.9000	0.8789
CNT-E-HM	681.96	4360.55	156.39	0.9300	0.9343

2.3. Surface Modification of CNTs. For acid modification, the as synthesized CNTs were sonicated for 1 hour and stirred using magnetic stirrer in room temperature with 4 M of HNO_3 acid for 24 hours [41, 42]. The CNTs were then washed with distilled water (until no pH changes occurred) and dried in oven for 24 hours at 100°C. For heat modification, the CNTs were put in the reactor and heated to 1000°C under argon flow for 1 hour. The modified CNTs produced from ethanol (CNT-E) and acetone (CNT-A) by acid and heat treatment are identified here as CNT-E-AM, CNT-A-AM, CNT-E-HM, and CNT-A-HM.

2.4. CNTs Characterization. The CNTs were characterized using VP-SEM (LEO 1455), TEM (Philips HMG 400), EDX (LEO 1455), and HRTEM (PHILIPS, TECNAI 2). Thermal analysis was performed using TGA/SDTA 851^e (METTLER-TOLEDO) under maximum temperature of 1000°C and heating rate of 5°C/min by inserting a small amount of CNTs (~10 mg) with an air flow rate of 10 mL/min. Samples were degassed prior to be used at 150°C for 12 hour under vacuum. Specific total surface areas were calculated using the BET equation, whereas specific total pore volumes were evaluated from nitrogen uptake at a relative pressure (P/P_0)

Table 6: The coefficients of the Langmuir, Freundlich, and Redlich-Peterson isotherms for phenol system.

(a)

CNTs	Langmuir isotherm			
	Q_m (mmol/kg)	K_L (L/mmol)	R_L (−)	R^2
CNT-A (as synthesized)	52.50	6.738	0.2227	0.8332
CNT-E (as synthesized)	120.38	25.04	0.0774	0.7489
CNT-A-AM	24.78	7.585	0.1936	0.7550
CNT-E-AM	58.60	2.99	0.3850	0.8156
CNT-A-HM	53.00	24.08	0.0745	0.6623
CNT-E-HM	181.09	12.87	0.1434	0.9757

(b)

CNTs	Freundlich isotherm			
	K_F (mmol/kg)/(mmol/L)$^{1/n}$	n	$1/n$	R^2
CNT-A (as synthesized)	57.31	2.0892	0.4787	0.8366
CNT-E (as synthesized)	145.56	3.7348	0.2675	0.9975
CNT-A-AM	25.85	2.6307	0.3801	0.5057
CNT-E-AM	52.34	1.8019	0.5549	0.8513
CNT-A-HM	57.86	4.9281	0.2029	0.5469
CNT-E-HM	216.38	2.7947	0.3578	0.9892

(c)

CNTs	Redlich-Peterson				
	A_R (L/g)	B_R (L/mmol)	q_{R-P} (mmol/kg)	β_R (−)	R^2
CNT-A (as synthesized)	0.51	46.45	10.9510	0.60	0.8956
CNT-E (as synthesized)	4.97	61.12	81.2698	0.90	0.9959
CNT-A-AM	0.18	7.67	24.5734	0.99	0.8489
CNT-E-AM	504189.30	13.55	3.72011	0.41	0.9333
CNT-A-HM	1.29	24.60	43.8880	0.99	0.9693
CNT-E-HM	5.59	82.13	68.0682	0.75	0.9979

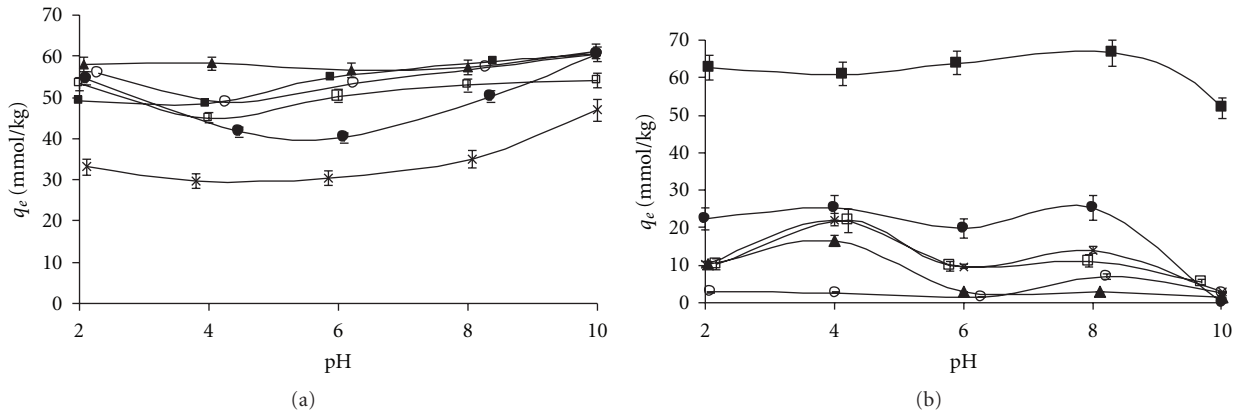

Figure 7: Effect of pH on (a) MB and (b) phenol adsorption capacity onto CNTs: ■ CNT-E-HM; • CNT-E (as synthesized); ▲ CNT-E-AM; × CNT-A (as synthesized); □ CNT-A-HM; ○ CNT-A-AM. Each point is the average value of triplicate samples. Error bars represent the range.

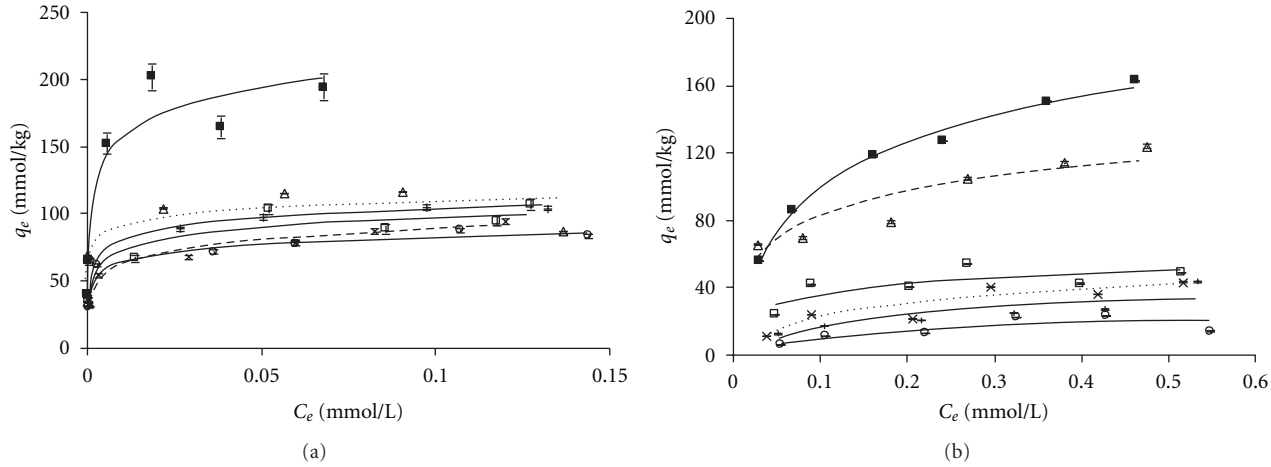

Figure 8: Plot of adsorption isotherm of (a) MB and (b) phenol onto CNTs: ■ CNT-E-HM; • CNT-E (as synthesized); ▲ CNT-E-AM; × CNT-A (as synthesized); □ CNT-A-HM; ○ CNT-A-AM. Each point is the average value of triplicate samples. Error bars represent the range.

Table 7: Comparison of the first-order, second-order and intraparticle diffusion rate constants values for MB adsorption on CNT-A-AM at different initial concentration.

(a)

C_0 (mmol/L)	Pseudo-first-order kinetic			
	$q_{e,\exp}$ (mmol/kg)	$q_{e,\text{calc}}$ (mmol/kg)	k_1 (min^{-1})	R^2
0.0156	27.02	18.13	0.0141	0.9712
0.0782	66.72	39.43	0.0113	0.9509
0.1563	72.28	40.26	0.0080	0.8853

(b)

C_0 (mmol/L)	Pseudo-second-order kinetic				
	$q_{e,\exp}$ (mmol/kg)	$q_{e,\text{calc}}$ (mmol/kg)	$q_{e,\exp}$ (mmol/kg)	R^2	$q_{e,\exp}$ (mmol/kg)
0.0156	27.02	27.94	0.002123	0.9931	1.5501
0.0782	66.72	67.53	0.009173	0.9718	4.1832
0.1563	72.28	69.94	0.000908	0.9394	4.4436

(c)

C_0 (mmol/L)	Intraparticle diffusion		
	k_i (mmol/kg/$\text{min}^{0.5}$)	C_i (mmol/kg)	R^2
0.0156	1.368	7.3303	0.9010
0.0782	3.171	20.1845	0.8775
0.1563	3.191	22.1716	0.8485

Table 8: Comparison of the first-order, second-order, and intraparticle diffusion rate constants values for MB adsorption on CNT-A-HM at different initial concentration.

(a)

C_0 (mmol/L)	Pseudo-first-order kinetic			
	$q_{e,\exp}$ (mmol/kg)	$q_{e,\text{calc}}$ (mmol/kg)	k_1 (min^{-1})	R^2
0.0156	29.24	8.94	0.0164	0.8205
0.0781	80.64	36.92	0.0152	0.9065
0.1563	110.96	34.87	0.0125	0.7755

(b)

C_0 (mmol/L)	Pseudo-second-order kinetic				
	$q_{e,\exp}$ (mmol/kg)	$q_{e,\text{calc}}$ (mmol/kg)	$q_{e,\exp}$ (mmol/kg)	R^2	$q_{e,\exp}$ (mmol/kg)
0.0156	29.24	28.07	0.0013	0.9900	10.1213
0.0782	80.64	81.63	0.0014	0.9819	9.5904
0.1563	110.96	110.87	0.0017	0.9760	21.1965

(c)

C_0 (mmol/L)	Intraparticle diffusion		
	k_i (mmol/kg/$\text{min}^{0.5}$)	C_i (mmol/kg)	R^2
0.0156	0.974	16.4302	0.4938
0.0782	3.498	34.2598	0.7114
0.1563	4.267	56.1451	0.6067

of N_2 equal to 0.99. The Barret, Johner, and Halenda (BJH) method was used to determine the distributions of the mesopores [43]. The zeta potential of CNTs was measured at pH 2–12 using a Zetasizer Nano Z (Malvern instrument). Seven measurements were made from each sample at each pH and the mean of zeta potential was determined as the point of isoelectric pH_{iep}.

The functional groups on the surface of CNTs were detected by a Fourier transform infrared (FTIR) spectroscopy (Nexus, Thermo Nicolet). The content of acidic and basic surface groups were obtained by titration [44]. The titration was conducted by adding 0.05 g of CNTs into a 100 mL flask containing 50 mL of the following 0.1 M solutions: $NaHCO_3$, Na_2CO_3, NaOH, and HCl. The flask was sealed and shaken at 25°C for 48 h, and then filtered through a 0.45 μm filter paper. The filtrate (10 mL) was pipetted and mixed with 0.1 M HCl. The excess acid was titrated with 0.1 M NaOH. The quantities of acidity of various types were determined

Table 9: Comparison of the first-order, second-order, and intraparticle diffusion rate constants values for phenol adsorption on CNT-A-AM at different initial concentration.

(a)

C_0 (mmol/L)	Pseudo-first-order kinetic			
	$q_{e,\exp}$ (mmol/kg)	$q_{e,\text{calc}}$ (mmol/kg)	k_1 (min^{-1})	R^2
0.0532	5.86	12.00	0.0050	0.6874
0.2656	42.55	22.36	0.0016	0.4109
0.5313	49.66	41.29	0.0023	0.9876

(b)

C_0 (mmol/L)	Pseudo-second-order kinetic				
	$q_{e,\exp}$ (mmol/kg)	$q_{e,\text{calc}}$ (mmol/kg)	k_2 (kg/mmol · min)	R^2	h (mg/g · min)
0.0531	5.86	3.46	0.001562	0.8157	0.1859
0.2656	42.55	34.28	0.001365	0.9103	1.6056
0.5313	49.66	40.68	0.000329	0.7982	0.5419

(c)

C_0 (mmol/L)	Intraparticle diffusion		
	k_i (mmol/kg/$\text{min}^{0.5}$)	C_i (mmol/kg)	R^2
0.0531	0.594	5.7815	0.6382
0.2656	1.117	14.2365	0.5577
0.5313	1.920	1.2953	0.8389

from the assumption that $NaHCO_3$ reacts with carboxylic groups, Na_2CO_3 reacts with carboxylic and lactonic groups, and NaOH reacts with carboxylic, lactonic, and phenolic groups.

2.5. Equilibrium Experiment. 100 mL of MB and phenol standard solution with predetermined initial concentration of 5, 10, 20, 30, 40, and 50 mg/L were put in the 250 mL conical flasks containing 0.05 g of CNTs. Those flasks with the mixture of CNTs and the adsorbates were completely wrapped with aluminum foil to prevent sunlight from causing color bleaching. The flasks were shaken using an orbital shaker, operated at 150 rpm at room temperature. The shaking process consummated for 72 hours. Then, the solution was centrifuged at 5000 rpm for 30 minutes. The clear supernatants were then decanted and analyzed using a UV-Vis spectrophotometer (Ultraspec 3100) at their maximum wavelength.

2.6. Kinetics Experiment. Kinetic experiments were performed at room temperature. CNTs (0.1 g) were introduced to 200 mL and 450 mL of MB and phenol solution, respectively, at optimum pH. Samples were taken at regular intervals and were analyzed using UV-Vis spectrophotometer. The quantity of the amount adsorbed at time t (min), q_t (mmol/kg), was calculated from

$$q_t = V \times \frac{(C_0 - C_t)}{m}, \quad (1)$$

where C_t is the concentration of solution at time t (mmol/L), C_0 is the initial concentration of solution at $t = 0$ (mmol/L), m is the CNTs weight (g), and V is the volume of solution (L).

3. Results and Discussion

3.1. Characterization of the CNTs. Figures 1(a) and 1(b) show the TEM images of the CNT-A-HM and CNT-E-HM respectively. No obvious physical change after surface modification is observed. Table 2 shows the physical properties of CNTs before and after surface modification. After acid modification, the surface area decreased as compared to as synthesized CNTs. As observed from the EDX analysis (Table 3), there is a reduction of Fe particles on CNTs after surface modification. It was found that acid and heat modifications contribute to the elimination of catalyst particles.

BET surface area also decreased for heat and acid-modified CNTs. This decrease maybe caused by the reduction of surface defect under high temperature as reported by Zhou et al. [45]. As for acid-modified CNTs, the formation of functional groups after oxidation blocks the pore of CNTs, thus, decreasing their pore volume. Similar result was also found by Lu et al. [46]. This observation is supported by FTIR result (shown in Figure 5), where many new oxygen functional groups were created after oxidation with HNO_3. For CNT-E, the heat treatment reduces the functional groups and hence increasing the total pore volume. Similar result was also reported by Shen et al. [24] and Chin et al. [47].

Figures 2(a) and 2(b) show N_2 adsorption isotherms for both adsorbent at 77 K. Acid-modified CNTs have a higher adsorption of N_2 than heat-modified CNTs. A steep increase of N_2 adsorption is observed below $(P/P_0) < 0.1$,

Table 10: Comparison of the first-order, second-order, and intraparticle diffusion rate constants values for phenol adsorption on CNT-A-HM at different initial concentration.

(a)

C_0 (mmol/L)	Pseudo-first-order kinetic			
	$q_{e,\exp}$ (mmol/kg)	$q_{e,\text{calc}}$ (mmol/kg)	k_1 (min^{-1})	R^2
0.0531	38.22	19.64	0.0115	0.7450
0.2656	54.49	24.64	0.0023	0.4109
0.5313	66.45	34.68	0.0026	0.5477

(b)

C_0 (mmol/L)	Pseudo-second-order kinetic				
	$q_{e,\exp}$ (mmol/kg)	$q_{e,\text{calc}}$ (mmol/kg)	k_2 (kg/mmol · min)	R^2	h (mg/g · min)
0.0531	38.22	42.23	0.002136	0.9981	3.8062
0.2656	54.49	47.35	0.001346	0.9540	3.0209
0.5313	69.32	57.13	0.000932	0.9470	3.0624

(c)

C_0 (mmol/L)	Intraparticle diffusion		
	k_i (mmol/kg/$\text{min}^{0.5}$)	C_i (mmol/kg)	R^2
0.0531	1.642	15.652	0.7029
0.2656	1.491	21.517	0.5564
0.5313	2.017	21.783	0.6751

enlarged in Figure 3, suggesting the presence of micropores. Heat-modified CNTs exhibit a type IV adsorption isotherm according to the IUPAC classification. A clear hysteresis indicating the production of mesopores. Modified CNT-A did not have high N_2 uptakes compared to as synthesized samples. CNT-E-AM has the highest N_2 uptakes, followed by as synthesized CNT-E, then CNT-E-HM. Based on pore size distribution in Figure 4, there are two major peaks at around 2–4 nm and 10 nm, and these two peaks decreased for modified CNT-A. However, for modified CNT-E, the volume decreased for pore size of 2–4 nm but no changes occurred for pore size of 10 nm.

3.2. Functional Group Analysis. Figure 5 presents the surface functional groups on the CNTs. After surface modification, CNTs became more hydrophilic and possessed more active functional groups hydroxyl (–OH), carboxylic acids and phenolic groups (O–H), and carbonyl groups (>C=O) at 3445, 1735, and 1400 cm^{-1}, respectively [48]. On the other hand, hydroxyl functional group is found to be reduced due to the decomposition of surface oxygen functional group under heat modification [49]. The increase of basic properties as quantified from the Boehm method for heat-modified CNTs is caused by basic groups for instance, pyrones and chromenes [50] and also electron-rich oxygen-free sites located on the carbon basal planes [51].

CNTs after acid modification had improved hydrophilic properties, making them more dispersed in water [52]. This improvement is due to the addition of oxygen functional groups as shown in Table 4. The total acidity increased approximately 44% and 40% for CNT-A and CNT-E, respectively. However, CNTs become more hydrophobic after heat treatment as indicated by their reduction in carboxyl functional group. Their total acidity decreased 40.3% and 19.26% for CNT-A and CNT-E, respectively. Heat modification reduces the oxygen functional groups on CNTs [53], activated carbon fiber [54], and graphite edge surface [55], as supported by the FTIR result shown in Figure 5.

3.3. Zeta Potential Analysis. Zeta potential of as synthesized CNTs and modified CNTs are shown in Figure 6. As the pH of solution increases, the zeta potential decreases. Under acid modification, the surface of CNT-A and CNT-E became acidic, that is, 5.9 and 4.2, respectively. Zeta potential of CNTs becomes more negative after oxidation, consistent with the results from Kuo [31] and Li et al. [56]. The pH_{iep} for CNT-A-HM and CNT-E-HM was 8 and 8.6, respectively, indicating the basic characteristics of both surfaces. The pH_{iep} of heat-treated CNTs is affected by the increment of basic sites (Table 4). Liu et al. [57], Karanfil, and Kilduff [58] reported that CNTs and activated carbon show basic characteristics, and reduction in polarity after heat treatment.

3.4. Adsorption Equilibrium

3.4.1. Optimum pH. Figures 7(a) and 7(b) show the effect of pH on adsorption of MB and Phenol onto modified CNT-A and CNT-E at initial concentration of 10 mg/L. For CNT-MB system, all modified CNTs have optimum pH of 10 which is caused by electrostatic interaction between the negative charge of their surface and positive charge of MB. The zeta potentials are at pH of 7.8, 5.9, 8, 8.6, 4.2, and 8.6, for

Table 11: Comparison of the first-order, second-order, and intraparticle diffusion rate constants values for MB adsorption CNT-E-AM at different initial concentration.

(a)

C_0 (mmol/L)	Pseudo-first-order kinetic			
	$q_{e,\exp}$ (mmol/kg)	$q_{e,\text{calc}}$ (mmol/kg)	k_1 (min^{-1})	R^2
0.0156	28.34	16.83	0.0180	0.9758
0.0781	105.41	95.09	0.0153	0.9045
0.1563	106.99	79.73	0.0117	0.9361

(b)

C_0 (mmol/L)	Pseudo-second-order kinetic				
	$q_{e,\exp}$ (mmol/kg)	$q_{e,\text{calc}}$ (mmol/kg)	k_2 (kg/mmol · min)	R^2	h (mg/g · min)
0.0156	28.34	29.49	0.002559	0.9788	2.2429
0.0782	105.41	113.28	0.000288	0.9897	3.7008
0.1563	106.99	110.87	0.000352	0.9841	4.1673

(c)

C_0 (mmol/L)	Intraparticle diffusion		
	k_i (mmol/kg/$\text{min}^{0.5}$)	C_i (mmol/kg)	R^2
0.0156	1.370	9.832	0.8338
0.0781	5.945	14.991	0.9696
0.1563	5.838	18.487	0.9331

CNT-A (as synthesized), CNT-A-AM, CNT-A-HM, CNT-E (as synthesized) CNT-E-AM, and CNT-E-HM, respectively.

The optimum pH for adsorption of phenol for as-synthesized CNT-A is at pH = 8 and for as-synthesized CNT-E is at pH = 4. Adsorption capacity is high at acidic environment due to dispersion interaction [38]. At this pH range, phenol is considered as neutral molecule. Above pH of 9.99, phenolate (anionic species) will dominate the solution, causing the repulsion interaction between negatively charged surfaces of CNT based on the zeta potential analyzer results (from −10 to −60 mV) as shown in Figure 6. This condition explains the decreasing of phenol being adsorbed as it approaches basic environment. Besides, the presence of OH^- ions on the adsorbents reduces the phenolate ions uptake [21, 39, 40].

3.4.2. Adsorption Isotherm. The equilibrium experimental data for adsorbed MB and phenol on modified CNTs were fitted using the adsorption isotherm equations, namely, Langmuir, Freundlich, and Redlich-Peterson. In this study, the best fit isotherm models to the experimental data were determined using the value of coefficient of determination, R^2 [59]

$$R^2 = \frac{\sum \left(q_{e,\text{cal}} - \overline{q_{e,\exp}}\right)^2}{\sum \left(q_{e,\text{cal}} - \overline{q_{e,\exp}}\right)^2 + \sum \left(q_{e,\text{cal}} - q_{e,\exp}\right)^2}, \quad (2)$$

where $q_{e,\text{cal}}$ is the equilibrium capacity obtained from isotherm model, $q_{e,\exp}$ is the equilibrium capacity obtained from experiment, and $\overline{q_{e,\exp}}$ is the average of $q_{e,\exp}$.

Besides the value of R^2, the applicability of equilibrium models was verified through the sum of squares error (SSE, %) [60]:

$$\text{SSE}(\%) = \sqrt{\frac{\sum \left(q_{e,\exp} - q_{e,\text{cal}}\right)^2}{N}} \times 100\%, \quad (3)$$

where N is the number of data.

3.4.3. Langmuir Isotherm. Langmuir isotherm [61] assumes that the single adsorbate binds to a single site on the adsorbent, and all the surface sites on the adsorbents have the same affinity for the adsorbate.

The equation is

$$q_e = \frac{Q_m K_L C_e}{1 + K_L C_e}, \quad (4)$$

where Q_m is the amount of adsorbate adsorbed per unit weight of adsorbent in forming a complete monolayer on the adsorbent's surface, q_e is the amount of adsorbate adsorbed per unit weight of adsorbent at equilibrium concentration, C_e, and K_L is the Langmuir constant.

The essential characteristics of the Langmuir isotherm can be described by a separation factor, defined by the following equation [62]:

$$R_L = \frac{1}{1 + K_L C_0}, \quad (5)$$

where R_L is the dimensionless equilibrium parameter, and C_0 is the initial adsorbate concentration.

Table 12: Comparison of the first-order, second-order, and intraparticle diffusion rate constants values for MB adsorption on CNT-E-HM at different initial concentration.

(a)

C_0 (mmol/L)	Pseudo-first-order kinetic			
	$q_{e,\exp}$ (mmol/kg)	$q_{e,\text{calc}}$ (mmol/kg)	k_1 (min^{-1})	R^2
0.0156	19.09	16.18	0.0191	0.9733
0.0782	42.63	47.90	0.0088	0.9123
0.1563	38.58	38.88	0.0104	0.8832

(b)

C_0 (mmol/L)	Pseudo-second-order kinetic				
	$q_{e,\exp}$ (mmol/kg)	$q_{e,\text{calc}}$ (mmol/kg)	k_2 (kg/mmol · min)	R^2	h (mmol/kg · min)
0.0156	19.09	19.76	0.019151	0.9780	7.4742
0.0782	42.63	41.14	0.008479	0.9920	14.3534
0.1563	38.58	35.68	0.011265	0.9680	14.3439

(c)

C_0 (mmol/L)	Intraparticle diffusion		
	k_i (mmol/kg/$\text{min}^{0.5}$)	C_i (mmol/kg)	R^2
0.0156	1.378	10.145	0.8067
0.0782	3.688	19.858	0.8682
0.1563	3.408	25.741	0.7939

Tables 5 and 6 summarize the adsorption isotherms plot in Figure 8. Heat-treated CNTs have the highest adsorption capacity for both systems. Adsorption process was favorable based on the separation factor, R_L between 0.0009 and 0.3850.

3.4.4. Freundlich Isotherm. The Freundlich model [63] is based on the distribution of adsorbate between the adsorbent and aqueous phases at equilibrium.

The basic Freundlich equation is

$$q_e = K_F(C_e)^{1/n}, \tag{6}$$

where K_F is the overall adsorption capacity, and $1/n$ is the heterogeneity factor that indicates the strength of bond energy between adsorbate and adsorbent.

CNT-E-HM has the highest adsorption capacity for MB and phenol. Based on $1/n$ values for both adsorbates, surface of CNT-A-HM is the most heterogeneous since its value is close to 0 [64].

3.4.5. Redlich-Peterson Isotherm. Redlich and Peterson model [65] represents the adsorption equilibrium over a wide concentration range of adsorbate. The adsorbate concentration at equilibrium condition is computed as follows:

$$q_e = \frac{K_R C_e}{1 + b_R(C_e)^{\beta_R}}, \tag{7}$$

where β_R, K_R, and b_R are constant parameters, normally, less than unity. This equation reduces to a linear isotherm at low surface coverage. In addition, at high adsorbate concentration, this equation will be equal to the Freundlich isotherm and when $\beta_R = 1$, it will be equal to the Langmuir isotherm.

The Langmuir and Redlich-Peterson isotherm fitted the experimental data for MB and phenol adsorption onto all adsorbents tested, respectively, as they have the highest R^2 and lowest SSE value.

3.5. Adsorption Kinetics. In the liquid phase adsorption process, the kinetic study is usually conducted to identify the kinetic reaction between the adsorbent and the adsorbate as well as the time required to achieve the maximum adsorption amount.

3.5.1. Pseudo-First-Order Kinetic. The pseudo-first-order kinetic model is given as [66]

$$\frac{dq_t}{dt} = k_1(q_e - q_t). \tag{8}$$

Integrating this equation for the boundary conditions $t = 0$ to $t = t$ and $q = 0$ to $q = q_t$ gives

$$\ln(q_e - q) = \ln q_e - k_1 t, \tag{9}$$

where q_t is the amounts of adsorbate adsorbed (mg/g) at time t (min), and k_1 is the rate constant of pseudo-first-order-adsorption (min^{-1}). The validity of the model is checked by linearizing the plot of $\ln(q_e - q_t)$ versus t where its slope is the rate constant of pseudo-first order adsorption. The values of k_1 and q_e at different initial concentration are presented in Tables 7, 8, 9, 10, 11, 12, 13, and 14. The

Table 13: Comparison of the first-order, second-order, and intraparticle diffusion rate constants values for phenol adsorption on CNT-E-AM at different initial concentration.

(a)

C_0 (mmol/L)	Pseudo-first-order kinetic			
	$q_{e,\exp}$ (mmol/kg)	$q_{e,\text{calc}}$ (mmol/kg)	k_1 (min^{-1})	R^2
0.0531	5.44	10.82	0.0103	0.8527
0.2657	45.25	23.63	0.0043	0.6548
0.5313	81.79	33.56	0.0037	0.4587

(b)

C_0 (mmol/L)	Pseudo-second-order kinetic				
	$q_{e,\exp}$ (mmol/kg)	$q_{e,\text{calc}}$ (mmol/kg)	k_2 (kg/mmol · min)	R^2	h (mmol/kg · min)
0.0531	5.44	5.12	5.12	0.002033	0.7377
0.2656	45.25	41.56	41.56	0.001299	0.9671
0.5313	81.79	74.67	74.67	0.001092	0.9747

(c)

C_0 (mmol/L)	Intraparticle diffusion		
	k_i (mmol/kg/$\text{min}^{0.5}$)	C_i (mmol/kg)	R^2
0.0531	4.657	3.100	0.8158
0.2656	20.206	14.201	0.7506
0.5313	19.841	34.175	0.5829

Table 14: Comparison of the first-order, second-order, and intraparticle diffusion rate constants values for phenol adsorption on CNT-E-HM at different initial concentration.

(a)

C_0 (mmol/L)	Pseudo-first-order kinetic			
	$q_{e,\exp}$ (mmol/kg)	$q_{e,\text{calc}}$ (mmol/kg)	k_1 (min^{-1})	R^2
0.0531	19.09	12.88	0.0067	0.8762
0.2656	42.63	15.77	0.0053	0.6746
0.5313	38.58	21.87	0.0420	0.7252

(b)

C_0 (mmol/L)	Pseudo-second-order kinetic				
	$q_{e,\exp}$ (mmol/kg)	$q_{e,\text{calc}}$ (mmol/kg)	k_2 (kg/mmol · min)	R^2	h (mmol/kg · min)
0.0531	19.09	19.76	0.0192	0.9780	7.4742
0.2656	42.63	41.14	0.0085	0.9920	14.3534
0.5313	38.58	35.68	0.0112	0.9680	14.3439

(c)

C_0 (mmol/L)	Intraparticle diffusion		
	k_i (mmol/kg/$\text{min}^{0.5}$)	C_i (mmol/kg)	R^2
0.0531	0.866	3.762	0.9202
0.2656	1.294	19.884	0.5596
0.5313	1.412	10.634	0.7810

correlation coefficient, R^2, is not high. Figures 9 and 10(a) show that the data only abides the model for the first 50 mins. According to Ho and McKay (1999) [67], the first-order kinetic model is generally applicable only over the initial stage of the adsorption processes.

3.5.2. Pseudo-Second-Order Kinetic. This model assumes that the differences between the average solid phase concentration at time t (min), q_t (mmol/kg), and the equilibrium concentration, q_e (mmol/kg), is the driving force for adsorption and the overall adsorption rate is proportional to the square of

Table 15: Previously reported adsorption capacities of various adsorbents for MB.

Adsorbent	Q_m (mmol/kg)	Reference
Pyrolyzed petrified sediment	7.47	Aroguz et al. [9]
Coir pith carbon	18.35	Kavitha and Namasivayam [10]
Salts-treated beech sawdust	30.33 ± 0.60–48.77 ± 2.40	Batzias and Sidiras [11]
Garlic peel	258.37–446.65	Hameed and Ahmad [12]
Activated desert plant	165.70	Bestani et al. [1]
Activated carbons	31.921–51.37	Karagöz et al. [13]
Wheat shells	51.77	Bulut and Aydin [14]
Spent coffee grounds	58.56	Franca et al. [15]
Acid treated-CNTs	110.68–202.28	Yao et al. [16]
As synthesized CNTs	**82.01–103.70**	**This work**
Acid-treated CNTs	**80.07–99.83**	**This work**
Heat-treated CNTs	**83.76–182.71**	**This work**

Table 16: Previously reported adsorption capacities of various adsorbents for phenol.

Adsorbent	Q_m (mmol/kg)	Reference
Corn grain-based activated carbons	2592.71	Park et al. [17]
Activated carbons	785.36–2530.02	Fierro et al. [18]
Physiochemical-activated coconut shell	2186.80	Mohd Din et al. [19]
Granular activated carbon	2529.91–2656.47	Hamdaoui and Naffrechoux [20]
Carbon cryogel microspheres	1312.29–2501.33	Kim et al. [21]
Acid-treated CNTs	386.78 ± 2.40–2380.19 ± 5.00	Lin and Xing [22]
Heated CNT	169.91	Diaz-Flores et al. [23]
Oxidized CNTs	436.72 ± 1.59	Shen et al. [24]
Acid-treated CNTs	168.74	Liao et al. [25]
As-synthesized CNTs	52.49–120.39	**This work**
Acid-treated CNT	24.76–58.55	**This work**
Heat-treated CNT	52.92–181.06	**This work**

the driving force [67]. The pseudo-second-order equation based on adsorption equilibrium capacity is expressed as [68]

$$\frac{dq_t}{dt} = k_1(q_e - q_t)^2. \tag{10}$$

Rearranging the variables in (10) gives

$$\frac{dq}{(q_e - q)^2} = k_2 dt. \tag{11}$$

Taking into account the boundary conditions $t = 0$ to $t = t$ and $q = 0$ to $q = q_t$, the integrated linear form of (11) can be rearranged to obtain(12)

$$\frac{t}{q} = \frac{1}{k_2 q_e^2} + \frac{t}{q_e}, \tag{12}$$

where k_2 is pseudo-second-order constant (kg/mmol/min) to be used to calculate the initial adsorption rate as below

$$h = k_2 q_e^2. \tag{13}$$

The values of q_e, k_2, and h obtained from this rate model at different concentration are given in Tables 7 to 14. The high R^2 value indicates that the experimental data fit the pseudo-second-order model. In conclusion, chemical adsorption might be the rate-limiting step, by either valent forces, through sharing of electrons between adsorbent and sorbate, or covalent forces, through the exchange of electrons between the parties involved [69]. The similar result also found using CNTs as adsorbents [16, 31, 70].

The pseudo-second-order constant is the highest for phenol-CNT-A which is $0.019151 \times$ kg/mmol · min, indicating the fastest mobility of phenol because the film resistance is small as shown by the boundary layer thickness, C_i from intraparticle diffusion model, 3.762 mmol/kg [71]. The molecular size of phenol is also smaller compared to MB as shown in Table 1. Based on the study of Lu et al. [72], smaller molecules diffused faster than the bigger ones. The rate constants of the pseudo-second-order model (k_2) decreased as the initial concentration of MB and phenol in adsorption systems increased. The same phenomenon was also reported by Kuo et al. [70], and Hameed and Rahman [73]. At lower concentration, the competition for the adsorption surface sites is lower compared to higher concentration.

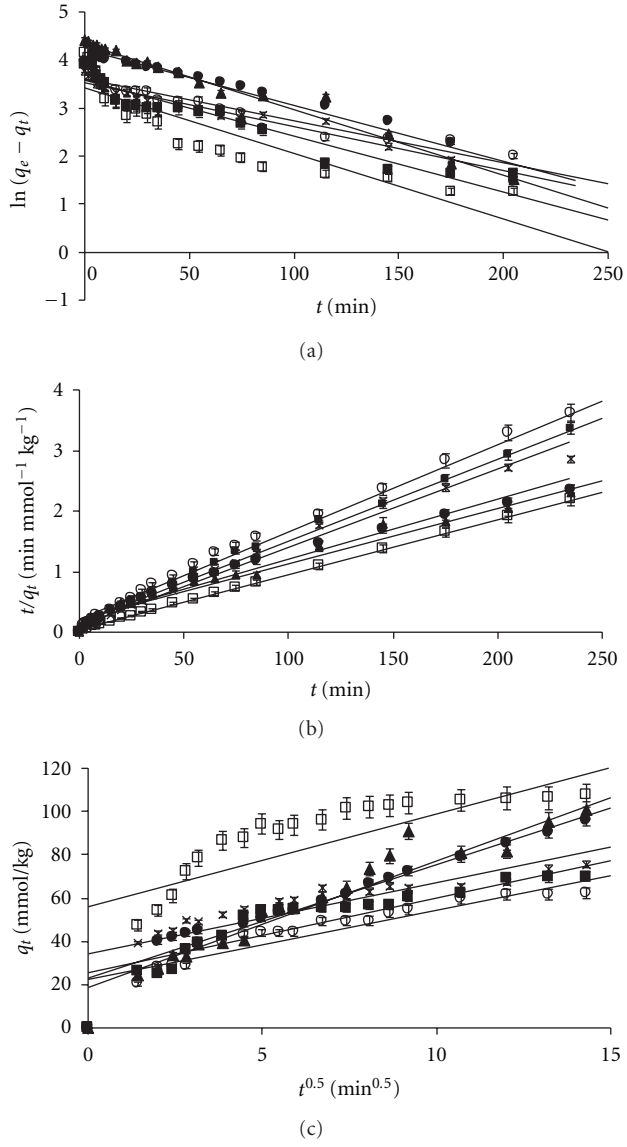

Figure 9: Plot of (a) pseudo-first-order-kinetic model, (b) pseudo-second-order-kinetic model, and (c) intraparticle diffusion model for the adsorption of 50 mg/L of MB onto CNTs. ■ CNT-E-HM; △ CNT-E (as synthesized); + CNT-E-AM; × CNT-A (as synthesized); □ CNT-A-HM; ◯ CNT-A-AM. Each point is the average value of triplicate samples. Error bars represent the range.

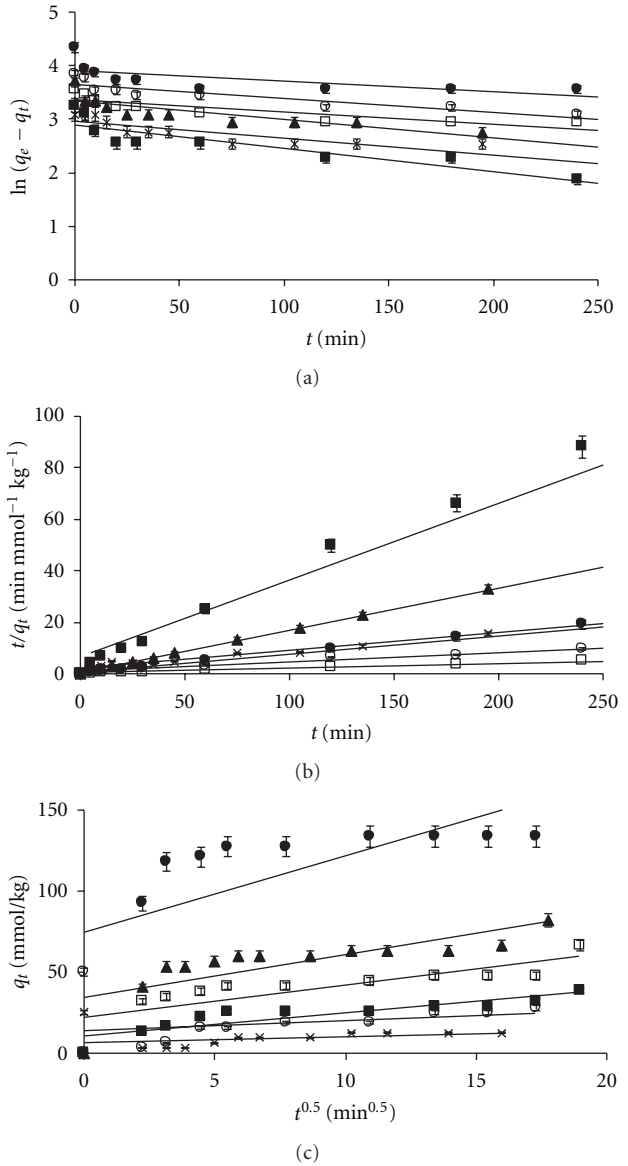

Figure 10: Plot of (a) pseudo-first-order-kinetic model, (b) pseudo-second-order-kinetic model, and (c) intraparticle diffusion model for the adsorption of 50 mg/L of phenol onto CNTs. ■ CNT-E-HM; △ CNT-E (as synthesized); + CNT-E-AM; × CNT-A (as synthesized); □ CNT-A-HM; ◯ CNT-A-AM. Each point is the average value of triplicate samples. Error bars represent the range.

3.5.3. Intraparticle Diffusion Kinetic. The intraparticle diffusion model to elucidate the diffusion mechanism is originally developed by Weber and Morris [74]

$$q_t = k_p t^{0.5} + C_i, \tag{14}$$

where C_i is the intercept, and k_p is the intraparticle diffusion rate constant (mg/g min$^{1/2}$), evaluated from the slope of the linearized plot of q_t versus $t^{1/2}$.

The regression plot of q_t versus $t^{0.5}$ in Figures 9(b) and 10(b) indicates linearity for all of the adsorbents tested, but it does not pass through the origin. This suggested that intraparticle diffusion was involved in adsorption, but it was not the only rate-controlling step.

3.6. Comparison of Adsorption Capacity. The maximum adsorption capacity of MB and phenol onto acid-modified CNTs decreased 3–9% as compared to as synthesized CNTs. For MB, there is an ionic repulsion between the CNTs modified with HNO_3 and MB [75]. The production of acidic oxygen functional groups on the CNTs surface (refer to Table 4) extracts the electrons from the π band of the carbon. As a result, the interaction between the MB molecules and the CNTs is reduced. The same result obtained for the adsorption

of MB onto acid-modified commercial activated carbons by Wang et al. [76] and Tan et al. [77].

The CNTs surface contains more acidic functional group with a decrease of hydroxide groups [76]. As for phenol, the increase of surface oxygen group, especially carboxylic group, makes the surface of acid-modified CNTs more hydrophilic. Through H bonding, the formation of water clusters negatively affects the accessibility and affinity of phenol, therefore, reducing the adsorption capacity [78, 79].

The more basic surface of the heat-treated CNTs promotes the high adsorption capacity of MB and phenol. For MB, the dispersive interactions between the π electrons on the surface of the basic carbon and the free electrons of the cationic dye molecule present in the aromatic rings and multiple bonds enhancing their adsorption [80]. As for phenol, adsorption mechanism of "donor-acceptor complex" contributes to its higher adsorption, where phenol acts as electron acceptor and basic surface of carbon acts as donor [66]. The adsorption capacities of MB and phenol on CNTs are as follows:

$$\text{Heat-treated CNTs} > \text{As synthesized CNTs} > \text{Acid-treated CNTs}. \quad (15)$$

Based on Tables 15 and 16, the adsorption capacities obtained in this study are comparable to various adsorbent and activated carbon, suggesting the potential usage of CNTs for wastewater treatment.

3.7. Comparison of Adsorption of MB and Phenol. In general, MB and phenol can adsorb well onto these types of CNTs. In MB system, the adsorption is enhanced by electrostatic interaction. As for phenol, the adsorption is dominated by π-π dispersion [81]. The molecular size of MB and phenol is small enough to enter the pore size of CNTs which are 3.28 and 2.42 nm for CNT-A and CNT-E, respectively. Furthermore, both the adsorbates structures are planar, which is beneficial for face-face conformation [82].

The MB adsorption onto the adsorbents is influenced by the mesopores whereas phenol adsorption is enhanced by the micropores [83]. Based on the N_2 adsorption isotherm as indicated in Figures 2(a) and 2(b), CNTs contain more mesopores. Therefore, the MB adsorption onto both adsorbents is higher than phenol adsorption. This work demonstrates that CNTs are suitable adsorbents for bigger molecular size adsorbate like MB compared to phenol as shown in Table 1.

4. Conclusion

A comparative study for different surface modifications of CNTs has been studied. The pseudo-second-order-kinetic model equation is the best to describe adsorption of MB and phenol on CNTs. Intraparticle diffusion was also identified to be one of the rate-controlling factors. By considering R^2 and SSE values, Langmuir and Redlich-Peterson isotherm fitted the experimental data for MB and phenol adsorption onto all adsorbents tested, respectively. Both surface modifications reduced the surface area of CNTs. The MB and phenol adsorption isotherms at room temperature show that the acid-modified CNTs have the lowest adsorption capacity, resulting from reduction in their surface area and the existence of abundant of surface oxygen functional groups. However, heat-treated CNTs have the highest adsorption capacity for MB and phenol, contributing by the basicity surface, in spite of their low surface area.

Acknowledgment

The authors are grateful for the financial support of Universiti Putra Malaysia (UPM).

References

[1] B. Bestani, N. Benderdouche, B. Benstaali, M. Belhakem, and A. Addou, "Methylene blue and iodine adsorption onto an activated desert plant," *Bioresource Technology*, vol. 99, no. 17, pp. 8441–8444, 2008.

[2] E. N. El Qada, S. J. Allen, and G. M. Walker, "Adsorption of methylene blue onto activated carbon produced from steam activated bituminous coal: a study of equilibrium adsorption isotherm," *Chemical Engineering Journal*, vol. 124, no. 1–3, pp. 103–110, 2006.

[3] E. Lorenc-Grabowska and G. Gryglewicz, "Adsorption characteristics of Congo Red on coal-based mesoporous activated carbon," *Dyes and Pigments*, vol. 74, no. 1, pp. 34–40, 2007.

[4] J. Seghatchian and P. Krailadsiri, "The quality of methylene blue treated FFP and cryo," *Transfusion and Apheresis Science*, vol. 25, no. 3, pp. 227–231, 2001.

[5] I. Arslan, I. A. Balcioglu, and D. W. Bahnemann, "Advanced chemical oxidation of reactive dyes in simulated dyehouse effluents by ferrioxalate-Fenton/UV-A and TiO2/UV-A processes," *Dyes and Pigments*, vol. 47, no. 3, pp. 207–218, 2000.

[6] A. N. M. Bagyo, H. Arai, and T. Miyata, "Radiation-induced decoloration and sedimentation of colloidal disperse dyes in water," *Applied Radiation and Isotopes*, vol. 48, no. 2, pp. 175–181, 1997.

[7] N. Saffaj, H. Loukili, S. A. Younssi et al., "Filtration of solution containing heavy metals and dyes by means of ultrafiltration membranes deposited on support made of Moroccan clay," *Desalination*, vol. 168, no. 1–3, pp. 301–306, 2004.

[8] M. Caetano, C. Valderrama, A. Farran, and J. L. Cortina, "Phenol removal from aqueous solution by adsorption and ion exchange mechanisms onto polymeric resins," *Journal of Colloid and Interface Science*, vol. 338, no. 2, pp. 402–409, 2009.

[9] A. Z. Aroguz, J. Gulen, and R. H. Evers, "Adsorption of methylene blue from aqueous solution on pyrolyzed petrified sediment," *Bioresource Technology*, vol. 99, no. 6, pp. 1503–1508, 2008.

[10] D. Kavitha and C. Namasivayam, "Experimental and kinetic studies on methylene blue adsorption by coir pith carbon," *Bioresource Technology*, vol. 98, no. 1, pp. 14–21, 2007.

[11] F. A. Batzias and D. K. Sidiras, "Dye adsorption by prehydrolysed beech sawdust in batch and fixed-bed systems," *Bioresource Technology*, vol. 98, no. 6, pp. 1208–1217, 2007.

[12] B. H. Hameed and A. A. Ahmad, "Batch adsorption of methylene blue from aqueous solution by garlic peel, an agricultural waste biomass," *Journal of Hazardous Materials*, vol. 164, no. 2-3, pp. 870–875, 2009.

[13] S. Karagöz, T. Tay, S. Ucar, and M. Erdem, "Activated carbons from waste biomass by sulfuric acid activation and their use on methylene blue adsorption," *Bioresource Technology*, vol. 99, no. 14, pp. 6214–6222, 2008.

[14] Y. Bulut and H. Aydin, "A kinetics and thermodynamics study of methylene blue adsorption on wheat shells," *Desalination*, vol. 194, no. 1–3, pp. 259–267, 2006.

[15] A. S. Franca, L. S. Oliveira, and M. E. Ferreira, "Kinetics and equilibrium studies of methylene blue adsorption by spent coffee grounds," *Desalination*, vol. 249, no. 1, pp. 267–272, 2009.

[16] Y. Yao, F. Xu, M. Chen, Z. Xu, and Z. Zhu, "Adsorption behavior of methylene blue on carbon nanotubes," *Bioresource Technology*, vol. 101, no. 9, pp. 3040–3046, 2010.

[17] K.-H. Park, M. S. Balathanigaimani, W.-G. Shim, J.-W. Lee, and H. Moon, "Adsorption characteristics of phenol on novel corn grain-based activated carbons," *Microporous and Mesoporous Materials*, vol. 127, no. 1-2, pp. 1–8, 2010.

[18] V. Fierro, V. Torné-Fernández, D. Montané, and A. Celzard, "Adsorption of phenol onto activated carbons having different textural and surface properties," *Microporous and Mesoporous Materials*, vol. 111, no. 1-3, pp. 276–284, 2008.

[19] A. T. Mohd Din, B. H. Hameed, and A. L. Ahmad, "Batch adsorption of phenol onto physiochemical-activated coconut shell," *Journal of Hazardous Materials*, vol. 161, no. 2-3, pp. 1522–1529, 2009.

[20] O. Hamdaoui and E. Naffrechoux, "Modeling of adsorption isotherms of phenol and chlorophenols onto granular activated carbon: part I. Two-parameter models and equations allowing determination of thermodynamic parameters," *Journal of Hazardous Materials*, vol. 147, no. 1-2, pp. 381–394, 2007.

[21] Y. A. Kim, H. Muramatsu, T. Hayashi, M. Endo, M. Terrones, and M. S. Dresselhaus, "Thermal stability and structural changes of double-walled carbon nanotubes by heat treatment," *Chemical Physics Letters*, vol. 398, no. 1–3, pp. 87–92, 2004.

[22] D. Lin and B. Xing, "Adsorption of phenolic compounds by carbon nanotubes: role of aromaticity and substitution of hydroxyl groups," *Environmental Science & Technology*, vol. 42, no. 19, pp. 7254–7259, 2008.

[23] P. E. Diaz-Flores, F. López-Urías, M. Terrones, and J. R. Rangel-Mendez, "Simultaneous adsorption of Cd^{2+} and phenol on modified N-doped carbon nanotubes: experimental and DFT studies," *Journal of Colloid and Interface Science*, vol. 334, no. 2, pp. 124–131, 2009.

[24] X.-E. Shen, X.-Q. Shan, D.-M. Dong, X.-Y. Hua, and G. Owens, "Kinetics and thermodynamics of sorption of nitroaromatic compounds to as-grown and oxidized multiwalled carbon nanotubes," *Journal of Colloid and Interface Science*, vol. 330, no. 1, pp. 1–8, 2009.

[25] Q. Liao, J. Sun, and L. Gao, "The adsorption of resorcinol from water using multi-walled carbon nanotubes," *Colloids and Surfaces A*, vol. 312, no. 2-3, pp. 160–165, 2008.

[26] W.-D. Zhang and W.-H. Zhang, "Carbon nanotubes as active components for gas sensors," *Journal of Sensors*, vol. 2009, Article ID 160698, 16 pages, 2009.

[27] E. T. Thostenson and T.-W. Chou, "Processing-structure-multi-functional property relationship in carbon nanotube/epoxy composites," *Carbon*, vol. 44, no. 14, pp. 3022–3029, 2006.

[28] S. H. Ng, J. Wang, Z. P. Guo, J. Chen, G. X. Wang, and H. K. Liu, "Single wall carbon nanotube paper as anode for lithium-ion battery," *Electrochimica Acta*, vol. 51, no. 1, pp. 23–28, 2005.

[29] A. D. Pasquier, H. E. Unalan, A. Kanwal, S. Miller, and M. Chhowalla, "Conducting and transparent single-wall carbon nanotube electrodes for polymer-fullerene solar cells," *Applied Physics Letters*, vol. 87, no. 20, Article ID 203511, pp. 1–3, 2005.

[30] Q. Liu, M. H. Nayfeh, and S.-T. Yau, "Brushed-on flexible supercapacitor sheets using a nanocomposite of polyaniline and carbon nanotubes," *Journal of Power Sources*, vol. 195, no. 21, pp. 7480–7483, 2010.

[31] C.-Y. Kuo, "Water purification of removal aqueous copper (II) by as-grown and modified multi-walled carbon nanotubes," *Desalination*, vol. 249, no. 2, pp. 781–785, 2009.

[32] J. Hu, C. Chen, X. Zhu, and X. Wang, "Removal of chromium from aqueous solution by using oxidized multiwalled carbon nanotubes," *Journal of Hazardous Materials*, vol. 162, no. 2-3, pp. 1542–1550, 2009.

[33] C. Lu and H. Chiu, "Adsorption of zinc(II) from water with purified carbon nanotubes," *Chemical Engineering Science*, vol. 61, no. 4, pp. 1138–1145, 2006.

[34] S. Zhang, T. Shao, S. S. K. Bekaroglu, and T. Karanfil, "Adsorption of synthetic organic chemicals by carbon nanotubes: effects of background solution chemistry," *Water Research*, vol. 44, no. 6, pp. 2067–2074, 2010.

[35] X. Xie, L. Gao, and J. Sun, "Thermodynamic study on aniline adsorption on chemical modified multi-walled carbon nanotubes," *Colloids and Surfaces A*, vol. 308, no. 1–3, pp. 54–59, 2007.

[36] J. Zhang, Z.-H. Huang, R. Lv, Q.-H. Yang, and F. Kang, "Effect of growing CNTs onto bamboo charcoals on adsorption of copper ions in aqueous solution," *Langmuir*, vol. 25, no. 1, pp. 269–274, 2009.

[37] X. Ren, C. Chen, M. Nagatsu, and X. Wang, "Carbon nanotubes as adsorbents in environmental pollution management: a review," *Chemical Engineering Journal*, vol. 170, no. 2-3, pp. 395–410, 2011.

[38] M. Pinault, M. Mayne-L'Hermite, C. Reynaud, O. Beyssac, J. N. Rouzaud, and C. Clinard, "Carbon nanotubes produced by aerosol pyrolysis: growth mechanisms and post-annealing effects," *Diamond and Related Materials*, vol. 13, no. 4–8, pp. 1266–1269, 2004.

[39] X. Peng, Y. Li, Z. Luan et al., "Adsorption of 1,2-dichlorobenzene from water to carbon nanotubes," *Chemical Physics Letters*, vol. 376, no. 1-2, pp. 154–158, 2003.

[40] C. Lu and H. Chiu, "Chemical modification of multiwalled carbon nanotubes for sorption of Zn2+ from aqueous solution," *Chemical Engineering Journal*, vol. 139, no. 3, pp. 462–468, 2008.

[41] V. Datsyuk, M. Kalyva, K. Papagelis et al., "Chemical oxidation of multiwalled carbon nanotubes," *Carbon*, vol. 46, no. 6, pp. 833–840, 2008.

[42] S. Gotovac, C.-M. Yang, Y. Hattori, K. Takahashi, H. Kanoh, and K. Kaneko, "Adsorption of polyaromatic hydrocarbons on single wall carbon nanotubes of different functionalities and diameters," *Journal of Colloid and Interface Science*, vol. 314, no. 1, pp. 18–24, 2007.

[43] E. P. Barrett, L. G. Joyner, and P. P. Halenda, "The determination of pore volume and area distributions in porous substances. I. Computations from nitrogen isotherms," *Journal of the American Chemical Society*, vol. 73, no. 1, pp. 373–380, 1951.

[44] H. P. Boehm, "Some aspects of the surface chemistry of carbon blacks and other carbons," *Carbon*, vol. 32, no. 5, pp. 759–769, 1994.

[45] J.-H. Zhou, Z.-J. Sui, P. Li, D. Chen, Y.-C. Dai, and W.-K. Yuan, "Structural characterization of carbon nanofibers formed from different carbon-containing gases," *Carbon*, vol. 44, no. 15, pp. 3255–3262, 2006.

[46] C. Lu, F. Su, and S. Hu, "Surface modification of carbon nanotubes for enhancing BTEX adsorption from aqueous

solutions," *Applied Surface Science*, vol. 254, no. 21, pp. 7035–7041, 2008.

[47] C.-J. M. Chin, L.-C. Shih, H.-J. Tsai, and T.-K. Liu, "Adsorption of o-xylene and p-xylene from water by SWCNTs," *Carbon*, vol. 45, no. 6, pp. 1254–1260, 2007.

[48] Y.-H. Li, C. Xu, B. Wei et al., "Self-organized ribbons of aligned carbon nanotubes," *Chemistry of Materials*, vol. 14, no. 2, pp. 483–485, 2002.

[49] P. C. C. Faria, J. J. M. Órfão, and M. F. R. Pereira, "Ozone decomposition in water catalyzed by activated carbon: influence of chemical and textural properties," *Industrial & Engineering Chemistry Research*, vol. 45, no. 8, pp. 2715–2721, 2006.

[50] U. Zielke, K. J. Hüttinger, and W. P. Hoffman, "Surface-oxidized carbon fibers: I. Surface structure and chemistry," *Carbon*, vol. 34, no. 8, pp. 983–998, 1996.

[51] C. A. Leon y Leon, J. M. Solar, V. Calemma, and L. R. Radovic, "Evidence for the protonation of basal plane sites on carbon," *Carbon*, vol. 30, no. 5, pp. 797–811, 1992.

[52] J. Li, S. Chen, G. Sheng, J. Hu, X. Tan, and X. Wang, "Effect of surfactants on Pb(II) adsorption from aqueous solutions using oxidized multiwall carbon nanotubes," *Chemical Engineering Journal*, vol. 166, no. 2, pp. 551–558, 2011.

[53] L. Ci, H. Zhu, B. Wei, C. Xu, and D. Wu, "Annealing amorphous carbon nanotubes for their application in hydrogen storage," *Applied Surface Science*, vol. 205, no. 1–4, pp. 39–43, 2002.

[54] S. Shin, J. Jang, S.-H. Yoon, and I. Mochida, "A study on the effect of heat treatment on functional groups of pitch based activated carbon fiber using FTIR," *Carbon*, vol. 35, no. 12, pp. 1739–1743, 1997.

[55] M. Nakahara, S. Asai, Y. Sanada, and T. Ueda, "Modification of oxidized graphite edge surface with poly(vinyl chloride)," *Journal of Materials Science*, vol. 30, no. 22, pp. 5667–5671, 1995.

[56] Y.-H. Li, S. Wang, Z. Luan, J. Ding, C. Xu, and D. Wu, "Adsorption of cadmium(II) from aqueous solution by surface oxidized carbon nanotubes," *Carbon*, vol. 41, no. 5, pp. 1057–1062, 2003.

[57] Z.-Q. Liu, J. Ma, Y.-H. Cui, L. Zhao, and B.-P. Zhang, "Influence of different heat treatments on the surface properties and catalytic performance of carbon nanotube in ozonation," *Applied Catalysis B*, vol. 101, no. 1-2, pp. 74–80, 2010.

[58] T. Karanfil and J. E. Kilduff, "Role of granular activated carbon surface chemistry on the adsorption of organic compounds. 1. Priority pollutants," *Environmental Science & Technology*, vol. 33, no. 18, pp. 3217–3224, 1999.

[59] K. V. Kumar and S. Sivanesan, "Isotherm parameters for basic dyes onto activated carbon: comparison of linear and non-linear method," *Journal of Hazardous Materials*, vol. 129, no. 1-3, pp. 147–150, 2006.

[60] B. H. Hameed, A. T. M. Din, and A. L. Ahmad, "Adsorption of methylene blue onto bamboo-based activated carbon: kinetics and equilibrium studies," *Journal of Hazardous Materials*, vol. 141, no. 3, pp. 819–825, 2007.

[61] I. Langmuir, "The adsorption of gases on plane surfaces of glass, mica and platinum," *The Journal of the American Chemical Society*, vol. 40, no. 9, pp. 1361–1403, 1918.

[62] T. W. Webi and R. K. Chakravorti, "Pore and solid diffusion models for fixed-bed adsorbers," *AIChE Journal*, vol. 20, no. 2, pp. 228–238, 1974.

[63] H. Freundlich, "Uber die adsorption in lunsungen," *Journal of Physical Chemistry*, vol. 57, pp. 387–470, 1985.

[64] F. Haghseresht and G. Q. Lu, "Adsorption characteristics of phenolic compounds onto coal-reject-derived adsorbents," *Energy & Fuels*, vol. 12, no. 6, pp. 1100–1107, 1998.

[65] O. Redlich and D. L. Peterson, "A useful adsorption isotherm," *Journal of Physical Chemistry*, vol. 63, no. 6, p. 1024, 1959.

[66] J. A. Mattson, H. B. Mark, M. D. Malbin, W. J. Weber, and J. C. Crittenden, "Surface chemistry of active carbon: specific adsorption of phenols," *Journal of Colloid And Interface Science*, vol. 31, no. 1, pp. 116–130, 1969.

[67] Y. S. Ho and G. McKay, "The sorption of lead(II) ions on peat," *Water Research*, vol. 33, no. 2, pp. 578–584, 1999.

[68] G. Blanchard, M. Maunaye, and G. Martin, "Removal of heavy metals from waters by means of natural zeolites," *Water Research*, vol. 18, no. 12, pp. 1501–1507, 1984.

[69] L. S. Oliveira, A. S. Franca, T. M. Alves, and S. D. F. Rocha, "Evaluation of untreated coffee husks as potential biosorbents for treatment of dye contaminated waters," *Journal of Hazardous Materials*, vol. 155, no. 3, pp. 507–512, 2008.

[70] C.-Y. Kuo, C.-H. Wu, and J.-Y. Wu, "Adsorption of direct dyes from aqueous solutions by carbon nanotubes: determination of equilibrium, kinetics and thermodynamics parameters," *Journal of Colloid and Interface Science*, vol. 327, no. 2, pp. 308–315, 2008.

[71] B. Cabal, C. O. Ania, J. B. Parra, and J. J. Pis, "Kinetics of naphthalene adsorption on an activated carbon: comparison between aqueous and organic media," *Chemosphere*, vol. 76, no. 4, pp. 433–438, 2009.

[72] C. Lu, Y.-L. Chung, and K.-F. Chang, "Adsorption thermodynamic and kinetic studies of trihalomethanes on multiwalled carbon nanotubes," *Journal of Hazardous Materials*, vol. 138, no. 2, pp. 304–310, 2006.

[73] B. H. Hameed and A. A. Rahman, "Removal of phenol from aqueous solutions by adsorption onto activated carbon prepared from biomass material," *Journal of Hazardous Materials*, vol. 160, no. 2-3, pp. 576–581, 2008.

[74] W. J. Weber and J. Morris, "Removal of biologically-resistant pollutants from waste waters by adsorption," in *Advances in Water Pollution Research*, Pergamon Press, New York, NY, USA, 1962.

[75] A. Rodríguez, G. Ovejero, J. L. Sotelo, M. Mestanza, and J. García, "Adsorption of dyes on carbon nanomaterials from aqueous solutions," *Journal of Environmental Science and Health, Part A*, vol. 45, no. 12, pp. 1642–1653, 2010.

[76] S. Wang, Z. H. Zhu, A. Coomes, F. Haghseresht, and G. Q. Lu, "The physical and surface chemical characteristics of activated carbons and the adsorption of methylene blue from wastewater," *Journal of Colloid and Interface Science*, vol. 284, no. 2, pp. 440–446, 2005.

[77] I. A. W. Tan, A. L. Ahmad, and B. H. Hameed, "Enhancement of basic dye adsorption uptake from aqueous solutions using chemically modified oil palm shell activated carbon," *Colloids and Surfaces A*, vol. 318, no. 1–3, pp. 88–96, 2008.

[78] M. Franz, H. A. Arafat, and N. G. Pinto, "Effect of chemical surface heterogeneity on the adsorption mechanism of dissolved aromatics on activated carbon," *Carbon*, vol. 38, no. 13, pp. 1807–1819, 2000.

[79] A. Dabrowski, P. Podkoscielny, Z. Hubicki, and M. Barczak, "Adsorption of phenolic compounds by activated carbon—a critical review," *Chemosphere*, vol. 58, no. 8, pp. 1049–1070, 2005.

[80] P. C. C. Faria, J. J. M. Órfão, and M. F. R. Pereira, "Adsorption of anionic and cationic dyes on activated carbons with different surface chemistries," *Water Research*, vol. 38, no. 8, pp. 2043–2052, 2004.

[81] S. Rengaraj, B. Arabindoo, V. Murugesan, and R. Sivabalan, "Adsorption kinetics of o-cresol on activated carbon from palm seed coat," *Indian Journal of Chemical Technology*, vol. 7, no. 3, pp. 127–131, 2000.

[82] C.-H. Liu, J.-J. Li, H.-L. Zhang, B.-R. Li, and Y. Guo, "Structure dependent interaction between organic dyes and carbon nanotubes," *Colloids and Surfaces A*, vol. 313-314, pp. 9–12, 2008.

[83] S. Altenor, B. Carene, E. Emmanuel, J. Lambert, J.-J. Ehrhardt, and S. Gaspard, "Adsorption studies of methylene blue and phenol onto vetiver roots activated carbon prepared by chemical activation," *Journal of Hazardous Materials*, vol. 165, no. 1–3, pp. 1029–1039, 2009.